Dictyostelium MEGAPs: F-BAR domain proteins that regulate motility and membrane tubulation in contractile vacuoles

Robert J. W. Heath[1,*] and Robert H. Insall[1,2]

[1]School of Biosciences, University of Birmingham, Edgbaston, Birmingham, B15 2TT, UK
[2]The Beatson Institute for Cancer Research, Glasgow, G61 1BD, UK
*Author for correspondence (e-mail: rjh451@bham.ac.uk)

Accepted 8 January 2008
Journal of Cell Science 121, 1054-1064 Published by The Company of Biologists 2008
doi:10.1242/jcs.021113

Summary

PCH family proteins are fundamentally important proteins, linking membrane curvature events with cytoskeletal reorganisation. One group, the MEGAPs (also called srGAPs and WRPs) contain RhoGAP domains in addition to the F-BAR domain. We disrupted MEGAP1 and MEGAP2 in *Dictyostelium* both singly and in combination. We found a strong cytoskeletal phenotype in MEGAP1$^-$ cells and a subtle phototaxis defect in MEGAP2$^-$ slugs. MEGAP1$^-$/2$^-$ cells have an overabundance of filopodia and slug motility and function are affected. The most dramatic changes, however, are on contractile vacuoles. MEGAP1$^-$/2$^-$ cells empty their contractile vacuoles less efficiently than normal and consequently have three times the usual number. GFP-tagged MEGAP1 localises to tubules of the contractile vacuole network and when vacuoles start to empty they recruit cytosolic GFP-MEGAP1. Mutants in the *Saccharomyces* homologues *RGD1* and *RGD2* also show abnormal vacuoles, implying that this role is conserved. Thus, MEGAP is an important regulator of the contractile vacuole network, and we propose that tubulation of the contractile vacuole by MEGAP1 represents a novel mechanism for driving vacuole emptying.

Supplementary material available online at
http://jcs.biologists.org/cgi/content/full/121/7/1054/DC1

Key words: Contractile vacuole, F-BAR, MEGAP, Rgd1, Tubulation

Introduction

Pombe/Cdc15 homology (PCH) family proteins are a group of adapter proteins prevalent in most eukaryotes, with the exception of plants. They have limited sequence identity but share similar domain architecture (Aspenstrom et al., 2006). PCH family proteins are identified as containing an N-terminal Fes/Cip4 homology (FCH) domain closely followed by a coiled-coil domain and a C-terminal SH3 (Src homology 3) domain (Lippincott and Li, 2000). The srGAP subfamily (Aspenstrom et al., 2006) also has a RhoGAP domain, usually located between the FCH and SH3 domains. Recent evidence demonstrates that the FCH domain and coiled-coil region actually constitute a larger F-BAR (FCH-Bin–amphiphysin–Rvs) domain (Itoh et al., 2005). Although the F-BAR domain remains a constant throughout, there is great variance in which other domains are present. Members of the PCH family include CIP4 (Aspenstrom, 1997), Toca1 (Ho et al., 2004), MEGAP (mental retardation GTPase-activating protein)/WRP (Endris et al., 2002; Soderling et al., 2002), NOSTRIN (Zimmermann et al., 2002), RGD1 (Barthe et al., 1998) and RGD2 (Roumanie et al., 2001).

The cellular functions of PCH family proteins are diverse. The yeast PCH family proteins are predominantly involved in actin reorganisation associated with cytokinesis (Lippincott and Li, 2000); one role of the RhoGAP-containing members is in low pH survival (Gatti et al., 2005). The srGAP subfamily has recently been identified (Wong et al., 2001) as being critically important in Slit-Robo signal transduction. SLIT proteins guide neuronal migration through roundabout (ROBO) transmembrane receptors. Slit increases binding of Robo1 to srGAP1, which, via increased GAP activity, inactivates Cdc42, inhibiting neuronal migration. The srGAP subfamily protein mental retardation GAP (MEGAP) is functionally inactivated in patients with the severe mental retardation disorder 3p$^-$ syndrome (Endris et al., 2002). Why the loss of MEGAP causes 3p$^-$ syndrome is unknown, but MEGAP is expressed in foetal and adult brain tissue (Endris et al., 2002) and may regulate cell migration (Yang et al., 2006), suggesting that the phenotypes of 3p$^-$ syndrome may be due to impaired neuronal migration and axonal connectivity.

MEGAP1 has previously been identified and named WAVE-associated RacGAP Protein (WRP) (Soderling et al., 2002). The SH3 domain of MEGAP is reported to bind to proline-rich sequences in SCAR1/WAVE1 and have Rac-specific GTPase activity (Soderling et al., 2002). Overexpression of MEGAP in cerebellar granular neurons reduces neurite outgrowth. Mice expressing a SCAR1/WAVE1 lacking the MEGAP-binding sites have reduced spine density, abnormal synaptic plasticity and memory defects (Soderling et al., 2007). This, in conjunction with the fact that SCAR1/WAVE1 null mice have behavioural phenotypes that overlap with symptoms of 3p$^-$ syndrome (Soderling et al., 2003), would suggest that WRP-mediated signalling through SCAR1/WAVE1 participates in regulation of the cytoskeleton underlying normal neuronal development.

The most commonly reported function of PCH family proteins in mammalian cells is of cytoskeletal organisation, often closely associated with the membranes (Aspenstrom et al., 2006). Activated Cdc42 interacts with the PCH family protein Toca1 and the N-WASP-WIP complex to bring about the activation of N-WASP, causing stimulation of actin nucleation via the Arp2/3 complex (Ho et al., 2004). The syndapin/PACSIN proteins have roles in both

membrane trafficking and reorganisation of the actin cytoskeleton (Kessels and Qualmann, 2004). Syndapin binds the GTPase dynamin, synaptojanin and N-WASP via the C-terminal SH3 domain and has an N-terminal F-BAR domain (Modregger et al., 2000; Kessels and Qualmann, 2004; Peter et al., 2004). The F-BAR domains of FBP17, CIP4 and syndapin are all capable of inducing membrane curvature associated with endocytosis (Itoh et al., 2005).

The contractile vacuole network is a paradigmatic membranous system, which undergoes tubular-vesicular transitions as part of its function as an osmoregulatory organelle (Gerisch et al., 2002). In *Dictyostelium discoideum* the contractile vacuole consists of an intracellular network of vacuoles and interconnecting tubules (Heuser et al., 1993). Tubules disappear as the vacuoles expand, by incorporation of the tubule membrane into the vacuole membrane (Heuser et al., 1993). In regulating the osmolarity of the cytosol, the contractile vacuole periodically fuses with the plasma membrane to expel water from the cell (Heuser et al., 1993). The membrane of the contractile vacuole network is distinct from that of the plasma membrane (Heuser, 2006) as it is decorated with vacuolar proton pumps driving the filling of the vacuole by transporting protons from the cytoplasm to the lumen (Heuser et al., 1993; Clarke et al., 2002). There is some evidence to suggest this may be ATP driven and regulated by P2X receptors (Fountain et al., 2007). Numerous proteins that regulate general membrane protein trafficking are important in contractile vacuole function (Gerisch et al., 2002). These proteins are often highly conserved in higher eukaryotes and thus relevant to trafficking pathways in mammalian systems.

The specific effects of genetic inactivation of PCH family proteins are poorly understood and there have been few attempts to understand the physiological implications from knockdown of PCH proteins. It is clear, however, that inactivation of PCH family genes can result in inflammatory disorders, mental retardation and cancer (Aspenstrom et al., 2006).

Here we describe two of the four RhoGAP family proteins in *D. discoideum*, which we have named MEGAP1 and MEGAP2. We have disrupted both *mgp1* and *mgp2* genes in AX3 cells by homologous recombination and made a *mgp1/2* double-knockout cell line. We find a morphological phenotype in *mgp1*$^{-}$ cells. *mgp1*$^{-}$*/2*$^{-}$ double mutant cells have an overabundance of filopodia and impaired motility. *mgp1*$^{-}$*/2*$^{-}$ cells have a severe contractile vacuole phenotype and the single knockouts have a subtler contractile vacuole phenotype. We therefore propose that MEGAP is a novel regulator of the contractile vacuole network.

Results

The *Dictyostelium* genome encodes six PCH family members

We have identified four genes encoding MEGAP-like proteins in the *Dictyostelium* genome project database, based on protein domain predictions from the SMART database (Schultz et al., 1998; Letunic et al., 2006). They are DDB0188795 (*gacBB*), DDB0190747 (*gacCC*), DDB0190412 (*gacAA*) and DDB0218546

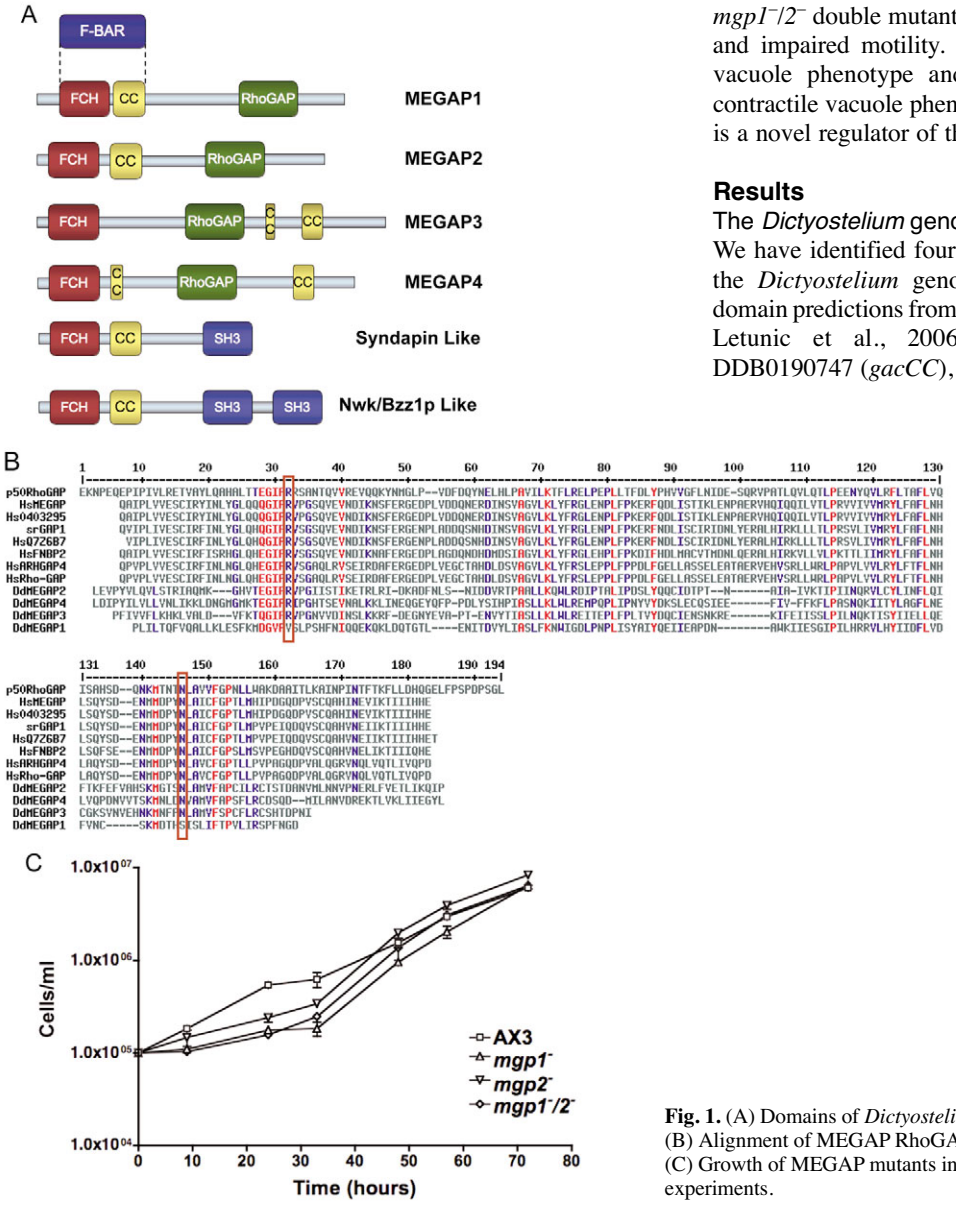

Fig. 1. (A) Domains of *Dictyostelium* MEGAPs as predicted by SMART db. (B) Alignment of MEGAP RhoGAP domains with known human GAP proteins. (C) Growth of MEGAP mutants in shaken culture. Data are mean ± s.e.m. of three experiments.

(*gacDD*; Fig. 1A). We would suggest that based on this work, more appropriate gene names would be *mgp1*, *mgp2*, *mgp3* and *mgp4*. Two further PCH family homologues were identified: DDB0203245 and DDB0168480. These genes encode proteins with N-terminal FCH and predicted coiled-coil domains and a C-terminal SH3 domain but no RhoGAP domains. Their domain organisations are similar to Syndapin (Qualmann et al., 1999) and Nwk/Bzz1p (Soulard et al., 2002; Coyle et al., 2004; Vlahou and Rivero, 2006), respectively (Fig. 1A).

MEGAP1, -2 and -4 have an N-terminal FCH domain closely followed by a predicted coiled-coil region, and a C-terminal RhoGAP domain (Fig. 1A). MEGAP3 however, has two predicted coiled-coil domains both of which are located at the C-terminus of the protein. *D. discoideum* MEGAPs, like the yeast homologues Rgd1 (Barthe et al., 1998) and Rgd2 (Roumanie et al., 2001), lack a C-terminal SH3 domain. The FCH and coiled-coil domains together have recently been described as a novel relative of the BAR domain, termed the F-BAR domain (Itoh et al., 2005), or EFC domain (Tsujita et al., 2006). These have further been grouped with other membrane-bending proteins, into the BAR domain superfamily (Frost et al., 2007).

The conserved residues Arg85 and Asn194, which are important in binding G proteins and essential for stimulating GTPase activity (Barrett et al., 1997), are present in MEGAP2, -3 and -4, but not MEGAP1 (Fig. 1B). This would suggest that MEGAP1 may not be a functional activator of GTPases and that MEGAP2, -3 and -4 could be functional activators of GTPases. MEGAP1 and MEGAP2 were chosen initially, as both are available from the Japanese cDNA project (Muramoto et al., 2003) and thus demonstrably expressed. We chose to apply the MEGAP nomenclature, as we can find no evidence of an association with SCAR/WAVE in *D. discoideum* (see below).

MEGAP-null cells have pleiotropic phenotypes

Both *mgp1* and *mgp2* genes were disrupted by homologous recombination in AX3 cells using blasticidin- and hygromycin-resistance cassettes, respectively. Disrupting *mgp2* with hygromycin in a blasticidin-resistant *mgp1*$^{-}$ background generated an *mgp1*$^{-}$/*2*$^{-}$ double mutant cell line. Gene disruptions were confirmed by Southern hybridisation (data not shown). Determination of vegetative growth rate in shaken suspension revealed no significant difference in doubling time between the MEGAP mutants and the parental AX3 strain (Fig. 1C) under these conditions.

Preliminary characterisation of MEGAP-null cells revealed that vegetative *mgp1*$^{-}$ cells have an obvious 'spiky' morphology (Fig. 2A), with an abundance of actin-rich filopodia (not shown) protruding from the cell membrane. *mgp2*$^{-}$ cells appear normal throughout vegetative growth and development (Fig. 2A). The *mgp1*$^{-}$/*2*$^{-}$ double mutant cells are generally ailing, displaying what appears to be an exaggerated phenotype. In vegetative growth

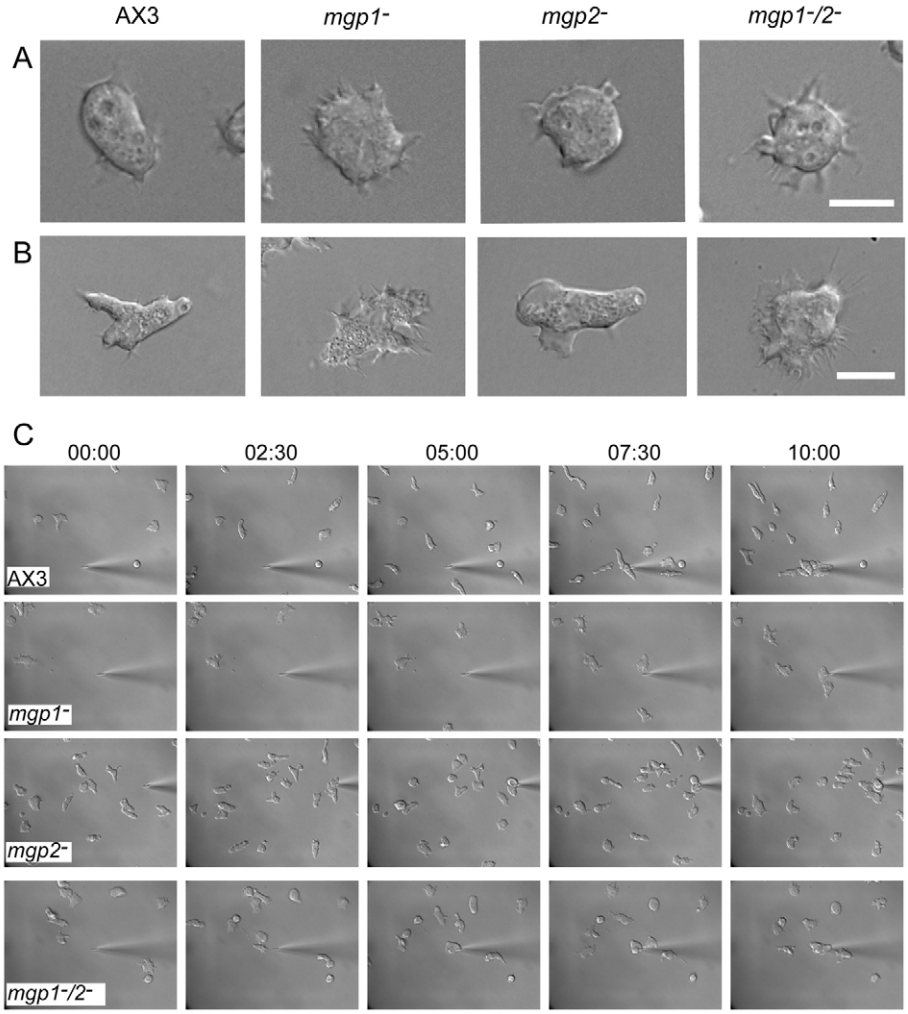

Fig. 2. MEGAP mutant morphology and chemotaxis. (A) Vegetative morphology of mutant and wild-type (AX3) cell lines during axenic growth. Axenically growing cells were observed using Nomarski differential interference contrast (DIC). (B) Developed morphology of cell lines during under-agar chemotaxis. Pulse developed cells were observed during under-agar chemotaxis to 100 nM cAMP. (C) Chemotaxis of respective cell lines to a point source of 1 μM cAMP. cAMP-pulsed AX3 and *mgp*$^{-}$ cells were resuspended in KK_2 medium and allowed to adhere to glass-bottomed dishes. Cells were then filmed for 10 minutes by DIC time-lapse microscopy, responding to a point source of cAMP delivered by micropipette. Images are representative of three experiments. Scale bars: 10 μm.

mgp1^{-}/*2*$^{-}$ cells appear spiky like *mgp1*$^{-}$ cells, and this spiky phenotype persists throughout early development (Fig. 2B). This is interesting because MEGAP1 may not have a catalytically functional GAP domain, in which case GAP activity must not be important for this phenotype.

Cell motility and chemotaxis

D. discoideum SCAR^{-} cells have abnormal actin distribution during chemotaxis (Bear et al., 1998), and both SCAR^{-} and PIR^{-} cells perform chemotaxis less efficiently than wild-type cells in under-agar chemotaxis experiments (Blagg et al., 2003). As MEGAP is a proposed negative regulator of SCAR (Soderling et al., 2002), we studied chemotaxis in MEGAP mutant cell lines to see whether they displayed any SCAR-related phenotype. *mgp*$^{-}$ cells are morphologically dissimilar to SCAR^{-} cells. SCAR-null cells are small and round (Bear et al., 1998) with decreased movement and chemotactic ability (Bear et al., 1998). Conversely, *mgp1*$^{-}$ and *mgp1*$^{-}$/*2*$^{-}$ cells are of a comparable size to the wild type and are covered in filopodia (Fig. 2A,B).

To investigate chemotaxis we subjected *mgp*$^{-}$ cells to a micropipette assay (Fig. 2C). The wild type and all three *mgp*$^{-}$ cell lines were capable of chemotaxing towards a point source of cAMP. However, both *mgp1*$^{-}$ and *mgp1*$^{-}$/*2*$^{-}$ cell lines were less efficient than wild-type cells in this assay. We observed that although all the parental AX3 cells in the field of view seemed to respond to the point source of cAMP, the *mgp*$^{-}$ cells at the periphery of the field were less efficient at responding to the cAMP point source (Fig. 2C). To quantify this observation, we measured average cell speed and chemotactic index of all the cell lines during under-agar chemotaxis experiments (Laevsky and Knecht, 2001). These revealed no significant difference in the chemotactic index of mutant cell lines relative to the wild type (Table 1). Cell speed, however, was affected in the mutant cell lines. Both *mgp1*$^{-}$ and *mgp1*$^{-}$/*2*$^{-}$ cells moved significantly slower than wild-type cells under these conditions. AX3 cells performed chemotaxis at an average speed of 10.6±0.75 μm/minute, whereas *mgp1*$^{-}$ and *mgp1*$^{-}$/*2*$^{-}$ cells were significantly slower at 8.16±0.6 and 8.07±0.36 μm/minute, respectively (P=0.0207 and P=0.0094). To test whether MEGAP1 interacts with SCAR we performed coimmunoprecipitations of the proteins. After many attempts to immunoprecipitate SCAR and probe for GFP-MEGAP1, or vice versa, we found no interaction between SCAR and MEGAP1 (data not shown). Taken together, these data demonstrate that MEGAP is essential for normal cell morphology and the slight difference in chemotaxis of *mgp1*$^{-}$ and *mgp1*$^{-}$/*2*$^{-}$ cells is probably due to a general motility defect.

Table 1. Chemotactic index and mean speed of *mgp* mutants during under agar chemotaxis

Cell line	Mean CI	Mean cell speed (μm/minute)
Control AX3	0.77±0.037	10.6±0.75
mgp1^{-}	0.75±0.047	8.16±0.6
mgp2^{-}	0.70±0.04	10.5±1.17
mgp1^{-}/*2*$^{-}$	0.79±0.024	8.07±0.36

Average cell speed and chemotactic index (CI) were determined from under-agar chemotaxis to cAMP experiments. Data are the mean of 10 cells from three experiments ± s.e.m. Chemotactic index is not significantly affected in the *mgp* mutants. Mean cell speed, however, is significantly reduced in *mgp1*$^{-}$ cells (P=0.0207) and *mgp1*$^{-}$/*2*$^{-}$cells (P=0.0094). *mgp2*$^{-}$ cells show no significant difference to the wild type (P=0.948).

Phototaxis and development

Multicellular development requires multiple aspects of cell movement, adhesion and contractility (Ibarra et al., 2006). To investigate the involvement of MEGAP in multicellular development we developed wild-type AX3 and all *mgp*-null strains on nitrocellulose membranes (Fig. 3A). *mgp1*$^{-}$ cells exhibited a marked defect, developing initially at the same rate as parental AX3 cells, but having fruiting bodies with smaller, thinner stalks (Fig. 3A). *mgp2*$^{-}$ cells develop morphologically normal fruiting bodies. The *mgp1*$^{-}$/*2*$^{-}$ double mutant has a severe fruiting defect (Fig. 3A), producing short fat stalks but rarely complete fruiting bodies. All the mutant cell lines proceeded through early development at the same rate as the wild-type cells. Aggregation on nutrient-free agar appeared to be reasonably consistent among the cell lines (Fig. 3B), although there were generally a larger number of cells not streaming in the *mgp1*$^{-}$ mutants, than any other cell line, and *mgp2*$^{-}$ aggregates could be larger than the wild type (Fig. 3B). In addition, the mound stage of *mgp1*$^{-}$ development lasted ~6 hours longer than in the wild type (not shown). When developing cells on nitrocellulose filters, we observed that *mgp*$^{-}$ slugs had more-prominent slug trails than wild-type slugs (not shown), suggesting that more cells are shed during migration. This is especially apparent in the *mgp2*$^{-}$ cell line. This observation prompted us to investigate slug behaviour of the *mgp*$^{-}$ cell lines.

The slug stage of the developmental cycle was affected in all the *mgp*$^{-}$ strains. After exposing slugs to a single point source of light for 48 hours, wild-type slugs were observed migrating toward the light source in a linear fashion (Fig. 3C). *mgp1*$^{-}$ slugs migrated a shorter distance with poor directionality. The trails of *mgp1*$^{-}$ slugs often showed sharp turns and sudden changes in direction (not shown) which we believe is consistent with slugs inappropriately rising up off the surface of the agar and then falling over and continuing to migrate in the direction they were orientated in upon landing. Movement of *mgp2*$^{-}$ slugs appeared less efficient than the wild type, but generally they still orientated correctly (Fig. 3C). The trails of *mgp2*$^{-}$ slugs often appeared denser than those of parental AX3 cells, suggesting a greater number of shed cells. *mgp1*$^{-}$/*2*$^{-}$ slugs displayed a more severe phenotype. Slugs of the double mutant were much less efficient at phototaxis (Fig. 3C) and frequently made the same sharp changes in direction displayed by *mgp1*$^{-}$ slugs. They were, however, more persistent than *mgp1*$^{-}$ slugs, achieving greater migration distances (Fig. 3C).

Close inspection of the slug stage revealed that all *mgp* mutant cells lines displayed a pronounced variability in slug length (Fig. 3D and Fig. 4). *mgp1*$^{-}$ cells made, on average, significantly shorter slugs than the wild type (Fig. 3D and Fig. 4; $P \leqslant 0.0001$). These slugs emerged much later than the wild type (~6 hours later), and were less persistent, moving onto the subsequent stages of development more readily. *mgp2*$^{-}$ slugs showed great variation in length (Fig. 3D and Fig. 4), with the mean being significantly greater than both wild-type and *mgp1*$^{-}$ slugs ($P \leqslant 0.0001$ in both instances). *mgp2*$^{-}$ cells develop into a few very large slugs (up to 1.7 mm long) and numerous smaller slugs (as short as 250 μm, Fig. 3D). These very long slugs probably account for the more-prominent trails observed on nitrocellulose membranes and may reflect the apparently larger aggregates (Fig. 3B). Interestingly, the slug stage of the double mutant was most similar to that of *mgp2*$^{-}$ cells. *mgp1*$^{-}$/*2*$^{-}$ slugs show a similar amount of variance in their length to the wild type (Fig. 3D and Fig. 4), but were, on average, significantly longer ($P \leqslant 0.0001$). They were also significantly

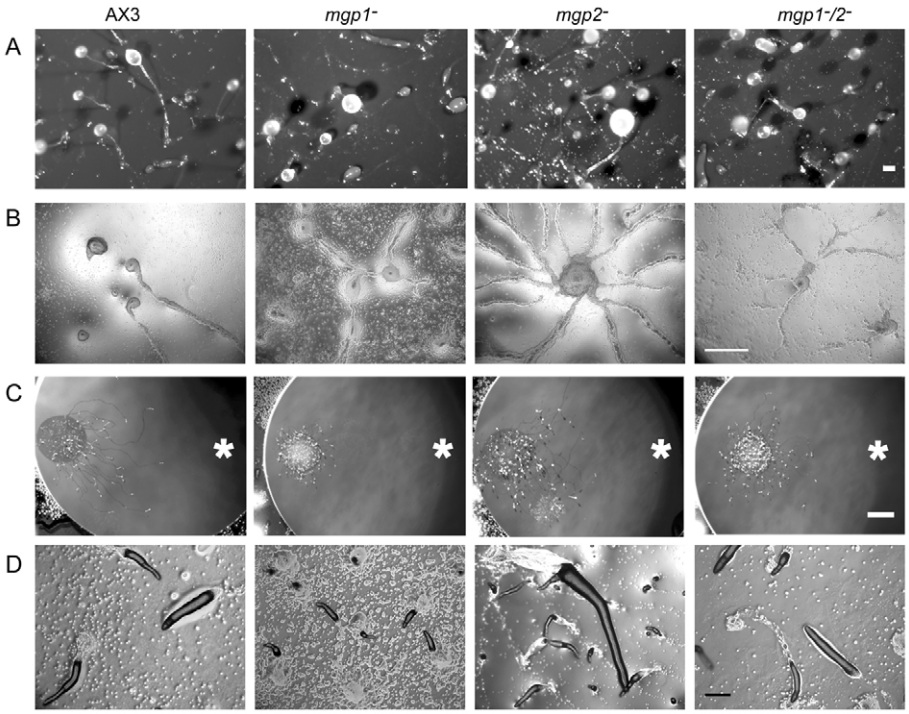

Fig. 3. MEGAP mutant phototaxis and development. (A) Terminal fruiting bodies of cell lines developed on nitrocellulose membranes for 48 hours. Scale bar: 2 mm. (B) Aggregation territories of cell lines on nutrient-free agar. A large quantity of nonstreaming cells can be observed in *mgp1* mutants. *mgp2* mutants often have larger aggregation centres than the wild type. Scale bar: 500 μm. (C) Phototaxis of slugs to a point light source. Light-directed migration of slugs after 48 hours on 0.5% charcoal agar shows that *mgp*$^{-}$ slugs are defective in phototaxis. Asterisks indicate the direction of the light source. Scale bar: 2 mm. (D) Representative examples of wild-type and *mgp* mutant slugs when cells are developed on nutrient-free agar. *mgp1*$^{-}$ slugs are shorter than the wild type and large clumps of cells remain on the substratum. *mgp2*$^{-}$ mutants form a few very large slugs and numerous shorter slugs. *mgp1*$^{-}$/*2*$^{-}$ slugs are also longer than wild-type slugs. Scale bar: 250 μm. Images are representative of three experiments.

longer than *mgp1*$^{-}$ slugs ($P \leqslant 0.0001$), but not *mgp2*$^{-}$ slugs ($P=0.7802$).

These data show that MEGAPs are involved in normal development. Whether failure to develop or perform phototaxis correctly is due to mechanical or sensory failure is unclear, but a mechanical explanation would seem more likely from these results.

MEGAP-null cells make excessive numbers of contractile vacuoles

Under axenic growth conditions, *mgp1*-null cells had a large number of vacuoles compared with the wild type, and *mgp1*$^{-}$/*2*$^{-}$ cells had even more (Fig. 5 and supplementary material Fig. S1). The most obvious vacuoles in *D. discoideum* are contractile vacuoles. The contractile vacuole network consists of interconnected tubular and vesicular elements and acts as an osmoregulatory organelle in fresh water and soil protozoa (Gerisch et al., 2002). All vacuoles are capable of fusing with the plasma membrane to discharge their contents. During discharge the contractile vacuole retains its identity, it collapses, flattens and tubulates but does not fully merge with the plasma membrane (Heuser, 2006).

To view the contractile vacuole network, we labelled cells with FM2-10 (Heuser et al., 1993). It was immediately apparent that both *mgp1*$^{-}$ and especially *mgp1*$^{-}$/*2*$^{-}$ cells had a strikingly larger number of contractile vacuoles than wild-type cells in these conditions (Fig. 5A, supplementary material Movie 1). To quantify this observation, we counted the number of contractile vacuoles per cell (Fig. 5B). The general range of vacuole numbers was significantly more varied in the mutant lines than in the parental line. All MEGAP mutant cell lines had, on average, more contractile vacuoles than the wild type (Fig. 4B inset), with *mgp1*$^{-}$ cells having twice as many and *mgp1*$^{-}$/*2*$^{-}$ having nearly three times as many contractile vacuoles as the parental strain. In particular, wild-type AX3 cells never appeared to have more than five contractile vacuoles, whereas the *mgp*-null cells could have as many as 14 contractile vacuoles at any one time (Fig. 5B). Observation of the tubular network suggested that the increased number of vacuoles arose at the expense of the tubules (supplementary material Fig. S2).

To ascertain the functional integrity of the contractile vacuole network, we assayed the osmosensitivity of the *mgp* double mutant. This mutant had the most-severe contractile vacuole phenotype and is therefore most likely to be osmotically sensitive. We were surprised to find that viability of the cells, following a severe osmotic shock (1 hour in water), was unaltered relative to the wild type (supplementary material Fig. S1). In addition, we tested the pH sensitivity of the *mgp* mutants by measuring growth at pH 5.0. We found no significant difference between the growth rates of the wild type and *mgp* mutants in these conditions (data not shown).

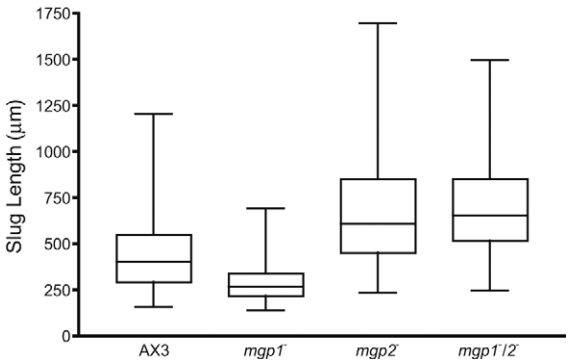

Fig. 4. MEGAP mutant slugs are significantly varied in length. Wild-type AX3 and *mgp* mutant cells were allowed to develop on nutrient-free agar plates. The length of at least 150 slugs from three experiments was measured and plotted as a box and whisker plot. *mgp1*$^{-}$ slugs (n=194) are significantly shorter than wild-type slugs (n=192; $P \leqslant 0.001$). *mgp2*$^{-}$ (n=151) and *mgp1*$^{-}$/*2*$^{-}$ (n=170) slugs are significantly longer than wild-type slugs ($P \leqslant 0.0001$ in both instances), but not significantly different from each other.

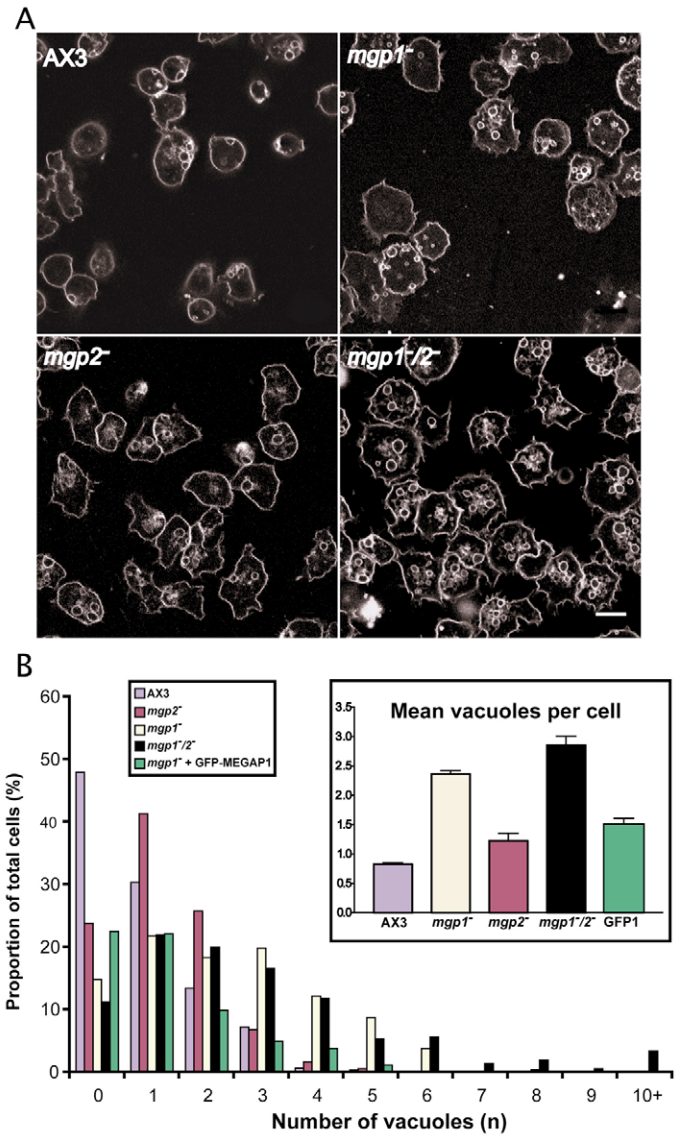

Fig. 5. Mutant MEGAP cells have more contractile vacuoles. (A) Contractile vacuole network of cells visualised with the lipophilic styryl dye FM2-10. Both *mgp1*$^{-}$ and *mgp1*$^{-}$*/2*$^{-}$ show many more contractile vacuoles than the wild type. Pictures are representative of at least three experiments. Scale bar: 10 µm. (B) Distribution of vacuole number in wild-type AX3 and *mgp*$^{-}$ cells visualised with FM2-10. Average number of vacuoles per cell ± s.e.m. is shown in inset. The number of vacuoles in each cell was counted for 30 minutes. The distribution in B reflects the frequency of cells containing (*n*) vacuoles for all cells over this time. *mgp1*$^{-}$ and *mgp1*$^{-}$*/2*$^{-}$ have, on average, significantly more contractile vacuoles than the wild type (P=0.0012 and P=0.0052, respectively). GFP-MEGAP1 expressed in the *mgp1*$^{-}$ background significantly rescues the contractile vacuole phenotype (P=0.0042).

We reasoned that the increased number of contractile vacuoles in *mgp*$^{-}$ cells could be the result of two possible causes: impaired emptying of contractile vacuoles or the production of more contractile vacuoles. To address these hypotheses we measured the total time taken to completely expel the contents of a contractile vacuole in wild-type and *mgp1*$^{-}$*/2*$^{-}$ cells, by live-cell imaging in hypo-osmotic conditions (Table 2). It took *mgp1*$^{-}$*/2*$^{-}$ cells 4 seconds longer than wild-type cells to empty each contractile vacuole. Although this figure is significant (P=0.0025) it is not nearly sufficient to account for the startling number of extra contractile vacuoles observed in *mgp*-null cells.

Table 2. Contractile vacuole expulsions are impaired in MEGAP mutants

Cell type	CV expulsion time (seconds)	Expulsions per CV
Control AX3	7.58±0.50	11.1
mgp1^{-}	7.82±0.46	–
mgp2^{-}	6.4±0.39	–
mgp1^{-}*/2*$^{-}$	10.12±0.74	7.5

Contractile Vacuole (CV) expulsion time is significantly slower (P=0.0025) in *mgp1*$^{-}$*/2*$^{-}$ cells, and each CV goes through fewer emptying cycles. Expulsion times were determined from under-agar DIC movies of vegetative cells in Lo Flo or one-third strength Lo Flo. Data is the average of 50 vacuoles from three experiments ± s.e.m. The number of expulsions per CV is inferred from the rate of CV expulsions in Fig. 6; it is the total number of CV expulsions (in 200 frames) divided by the average number of CVs per cell.

Since the impaired expulsion time of *mgp*-null contractile vacuoles does not fully explain the increased contractile vacuole number, we hypothesised that impairment of the contractile vacuole expulsion rate (the number of expulsion events in a measured time) could be a contributing factor. To address this question, we labelled cells with FM2-10 and tallied the number of contractile vacuole expulsions per cell over 20 minutes by confocal microscopy (Fig. 6A). We found that the rate of contractile expulsion events was unaffected in *mgp1*$^{-}$*/2*$^{-}$ cells (Fig. 6A). By counting the average number of contractile vacuoles per cell in these conditions, we were also able to infer the number of times each contractile vacuole is expelled (Table 2). Wild-type cells expelled each vacuole ~11.12 times per 20 minutes, whereas *mgp1*$^{-}$*/2*$^{-}$ cells expelled each vacuole only 7.5 times in 20 minutes.

In addition, we considered whether the general activation of Rac in these cells would affect the rate of contractile vacuole expulsion events. To test this we repeated the previous experiment, but treated cells with a large (25 µM) folate stimulus (to generally activate Rac) after 8 minutes (Fig. 6B). Stimulation of AX3 and *mgp1*$^{-}$*/2*$^{-}$ with folate had no effect on the rate of contractile vacuole expulsions. This suggests that the rate of contractile vacuole expulsion events observed represents the minimum expulsion rate required for cell survival in these conditions. It further suggests that in order to meet this rate threshold, *mgp1*$^{-}$*/2*$^{-}$ cells have to make around three times as many contractile vacuoles to compensate; or conversely, if the mutation leads to an increased number of vacuoles, they need to empty less frequently to keep up with water influx. However, the localisation of GFP-MEGAP1 at the beginning of vacuole expulsion, suggests MEGAP1 is functional in emptying, supporting the first argument.

GFP-MEGAP1 localises to the contractile vacuole

To further investigate the role of MEGAPs in *D. discoideum*, we expressed N-terminal GFP-tagged full-length MEGAP1 in the single-knockout background. Under normal axenic growth conditions, GFP-MEGAP1 labelled the tubular network of the contractile vacuole (Fig. 7A). A proportion was also cytosolic. To stimulate contractile vacuole activity we incubated cells in growth medium diluted 1:3 in water for 30-60 minutes before imaging. Under these conditions, GFP-MEGAP1 migrated predominantly to the cytosol. GFP-MEGAP1-labelled vesicles transiently localised to expelling vacuoles just after emptying had begun (Fig. 7B,

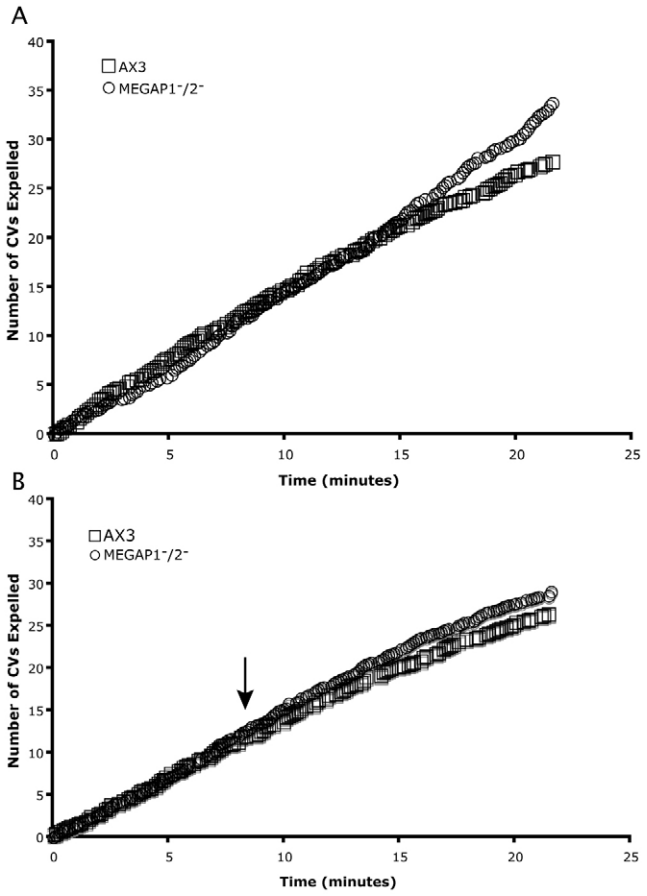

Fig. 6. The rate of contractile vacuole expulsion is unaffected in *mgp1*$^{-}$/2^{-} cells. (A) Average contractile vacuole (CV) expulsions rate of wild-type AX3 (squares) and *mgp1*$^{-}$/2^{-} cells (circles). (B) Average contractile vacuole expulsions rate of AX3 (squares) and *mgp1*$^{-}$/2^{-} (circles) when stimulated with 25 μM folate (arrow). Each point of the graph represents the cumulative average number of vacuole expulsions in ten cells (from three experiments) over time. The slope therefore reflects the average rate of vacuole expulsion events.

supplementary material Movie 2). Complete emptying of the vacuoles could be seen as a bright patch of GFP that then seemed to diffuse back into the cytosol. Interestingly, a proportion of GFP-MEGAP1 often remained bound to the tubules formed from the emptying contractile vacuole (Fig. 7A, supplementary material Movie 3), where it remained until the vacuole refilled. We also observed GFP-MEGAP1-labelled puncta travelling along the tubular network from one expelling bladder to the next.

Localisation of GFP-MEGAP1 to the tubular network of the contractile vacuole under iso-osmotic conditions, or puncta that associate with the contractile vacuole membrane when emptying, under hypo-osmotic conditions, suggests that MEGAP1 functions in tubulating the expelling vacuole. Expression of GFP-MEGAP1 in the *mgp1*$^{-}$ background significantly reduced the vacuole number in hypo-osmotic conditions to near wild-type levels (Fig. 5B, P=0.0042) but did not rescue the cytoskeletal phenotype (not shown).

Macropinocytosis is unaffected in MEGAP mutants

The contractile vacuole is a post-Golgi compartment that shares a common origin with the endo-lysosomal system (Gabriel et al., 1999). However, the contractile vacuole remains separate from vesicles of the endosomal pathway. We were intrigued as to whether MEGAP1 also plays a role in vesicle trafficking. In *Dictyostelium*, macropinocytosis accounts for the majority of fluid-phase uptake (Hacker et al., 1997). If MEGAPs were affecting general membrane curvature in *D. discoideum* we would postulate that macropinocytosis (which requires large changes in membrane curvature) might be affected. To test this hypothesis we measured uptake of the fluid phase marker TRITC-dextran in wild-type and MEGAP-null cells (Fig. 8). There was no significant difference in the ability of *mgp*$^{-}$ cells to perform macropinocytosis when measured fluorimetrically (Fig. 8A) or when observed by live-cell microscopy (Fig. 8B). Although there may be some redundancy between the MEGAPs, this strongly suggests that MEGAP1 and MEGAP2 in *D. discoideum* are not important in altering membrane curvature during macropinocytosis.

Mutant yeast orthologues *Rgd1* and *Rgd2* display abnormal vacuoles

Rgd1p and Rgd2p are the yeast orthologues of MEGAP. *Rgd1Δ* cells have a small growth defect in minimal medium and accumulate GTP-bound Rho3p and Rho4p, but are otherwise normal (Barthe et al., 1998). The *Rgd1Δ* mutant is sensitive to medium acidification (Gatti et al., 2005). Given the high degree of similarity between Rgd1p and *D. discoideum* MEGAP we hypothesised that *Rgd1Δ* and *Rgd2Δ* cells might also have a vacuole phenotype. We labelled *Rgd1Δ* and *Rgd2Δ* cells with the lipophilic membrane dye FM4-64 and observed them using epifluorescence microscopy (Fig. 9). When compared with the wild-type parental strain BY4322, both *Rgd1Δ* and *Rgd2Δ* cells had more vacuoles. The vacuoles in *Rgd1Δ* cells were smaller and more numerous than those of the wild type (Fig. 9, arrows). *Rgd2Δ* cells generally had clusters of smaller vacuoles (Fig. 9, arrows).

This suggests that the abnormal behaviour of vacuoles in *Rgd1Δ* may contribute to the pH-sensitivity phenotype. The abnormal vacuole number of *Rgd2Δ* cells is consistent with Rgd2p interacting with Cdc42p, because Cdc42p is required for vacuole fusion and normal vacuole copy number in yeast (Eitzen et al., 2001). The yeast vacuole is a complex organelle. In addition to being involved in lysosomal processes, it is also involved in osmoregulation and precise homeostatic regulation of cytosolic ion concentration and pH (Klionsky et al., 1990). The phenotypes observed in both *Rgd* mutant cell lines are strikingly similar to those observed in the MEGAP mutants and the yeast vacuole has functions in common with the contractile vacuole network of *D. discoideum*. These data suggest that the roles of MEGAP proteins are evolutionarily conserved.

Discussion

We have identified six PCH family genes encoding F-BAR-domain-containing proteins in the genome of *D. discoideum* (Eichinger et al., 2005). Four of these contain a RhoGAP domain; the other two contain SH3 domains. We have named the RhoGAP members MEGAP and characterised the physiological roles of MEGAP1 and MEGAP2. Our results show that both MEGAP1 and MEGAP2 are involved throughout the *D. discoideum* life cycle.

To perform functional analyses, knockout cell lines were created for both *mgp1* and *mgp2* by homologous recombination. Pleiotropic phenotypes were apparent. *mgp1*$^{-}$ cells had a distinct morphological phenotype characterised by an overabundance of surface protrusions. The distinct surface protrusions of *mgp1*$^{-}$ cells were

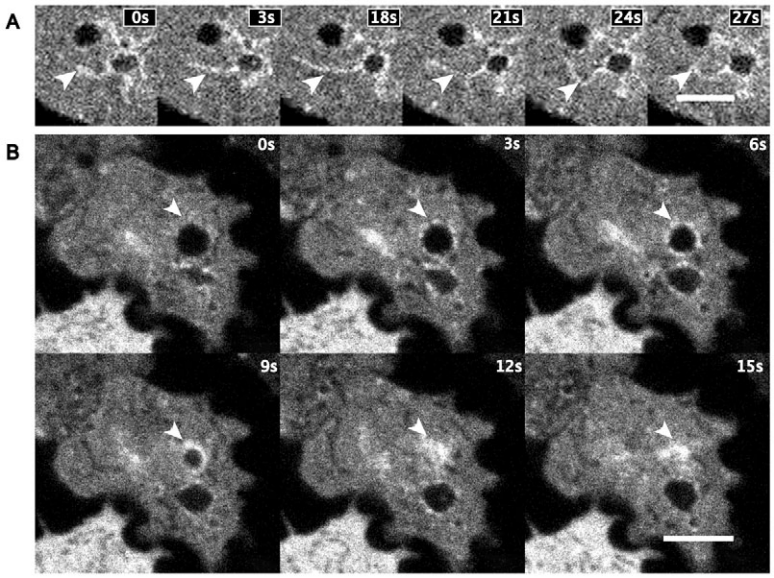

Fig. 7. GFP-MEGAP1 labels the contractile vacuole network. (A) GFP-MEGAP1 localises to tubules associated with the contractile vacuole membrane in an iso-osmotic environment (arrowheads). (B) Live imaging of GFP-MEGAP1-expressing cells in a hypo-osmotic environment reveals transient localisation to contractile vacuoles at the point of discharge, suggesting that MEGAP1 is important in contractile vacuole emptying. Contractile vacuole activity was stimulated by incubating cells for 30 minutes in Lo Flo. Cells were imaged using an agar-overlay technique (Yumura et al., 1984) by confocal microscopy. Scale bars: 5 μm.

similar to those observed in cells lacking the IQGAP-related protein DGAP1 (Faix et al., 1998), and cells overexpressing GFP-Rac1A, GFP-Rac1B and GFP-Rac1C (Dumontier et al., 2000). DGAP1 is a Rac1A-binding protein and is involved in modulating the F-actin cytoskeleton and controlling cell motility. Expression of constitutively active GFP-Rac1A, -Rac1B or -Rac1C in cells induces the formation of numerous long dynamic filopodia. The RhoGAP domain of MEGAP1 does not contain the essential amino acids Arg85 or Asn194 and is thus expected not to function as a GTPase-activating protein. This suggests that MEGAP1 is more likely a downstream effector of RhoGTPases than an activator per se. *mgp1*$^{-}$ cells can perform chemotaxis to a point source of cAMP at a rate comparable with the wild type, but cells at the periphery were less efficient at responding to the signal.

mgp1^{-} slugs showed apparent poor directionality when phototaxing to a light source (Fig. 3C) and the terminal fruiting bodies were borne on shorter and thinner stalks than those of the wild type. A closer inspection of aggregation and the slug stage reveals that *mgp1*$^{-}$ cells make much shorter slugs that are less persistent than the wild type (Fig. 3D and Fig. 4). In addition, a large number of cells remained separate from aggregation centres and slugs (Fig. 3B,D). The precise cause of this is unclear; one possible explanation is that the greatly increased surface protrusions of the *mgp1* mutants cause greater cell-substrate adhesion, which is reflected in the slower chemotaxis speeds of *mgp1*$^{-}$ cells (Table 1). An increased cell-substrate adhesion may detrimentally affect the cell-cell adhesions required for slug formation, subsequently resulting in short slugs. Smaller slugs would account for the generally smaller fruiting bodies and the apparent phototaxis defect is more likely to be a mechanical failure of slug formation.

The lack of an obvious phenotype during vegetative growth of *mgp2*$^{-}$ cells would suggest that MEGAP2 is either not important at this stage of the life cycle or that functional redundancy exists between the various family members. The latter seems more likely. An element of compensation may also exist. *mgp2*$^{-}$ slugs also showed significant variation in mean length. The more prominent slug trails of *mgp2*$^{-}$ may be due to the much larger slugs having a more prominent slime sheath than the wild-type cells (Fig. 3D).

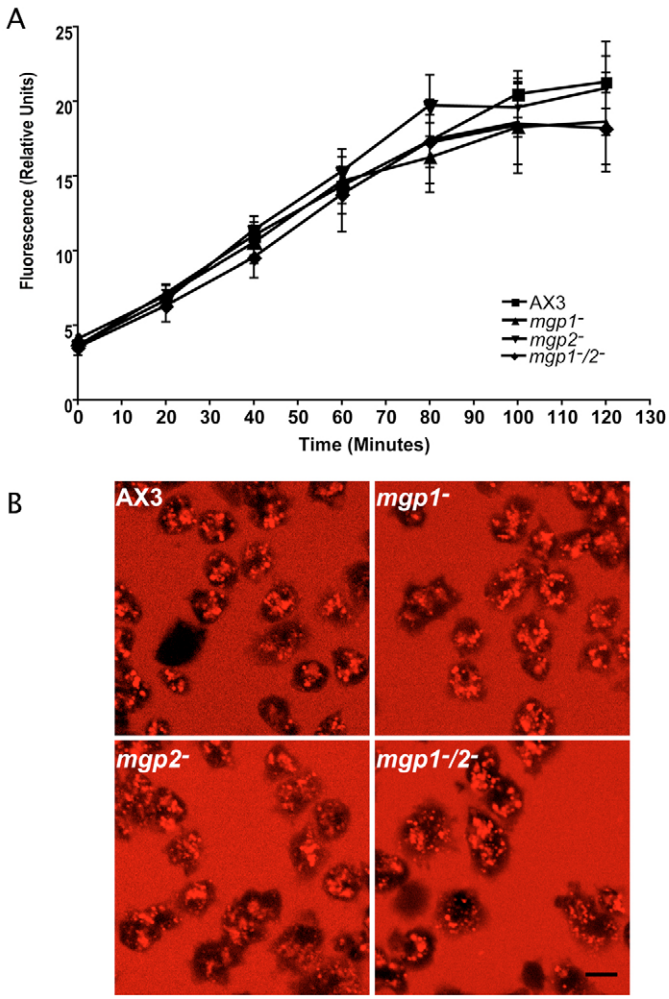

Fig. 8. Macropinocytosis is unaffected in MEGAP mutants. (A) Quantification of fluid-phase uptake. The rate of fluid-phase uptake is unaltered in MEGAP mutants. Mean ± s.e.m. of three experiments. (B) Visualisation of fluid-phase uptake. Confocal images showing normal TRITC-dextran internalisation in MEGAP mutant cell lines. Scale bar: 10 μm.

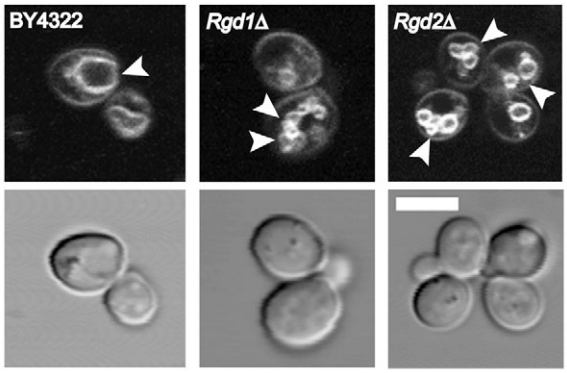

Fig. 9. *S. cerevisiae* Δ*Rgd1* and Δ*Rgd2* cells have numerous small vacuoles. Cells were labelled with FM4-64 dye and visualised by confocal microscopy. Both *Rgd1*Δ and *Rgd2*Δ lines have a greater number of vacuoles (arrowheads), which are smaller than those in the wild type. Scale bar: 5 μm.

The *mgp1*$^{-}$/*2*$^{-}$ phenotype is generally more pronounced than that in either of the single gene disruption cell lines. In vegetative growth, *mgp1*$^{-}$/*2*$^{-}$ cells had the same spiky appearance as *mgp1*$^{-}$ cells and this spiky phenotype persisted through early development. The *mgp1*$^{-}$/*2*$^{-}$ double mutant had severe defects in both slugs and fruiting bodies. Interestingly the slug phenotype of *mgp1*$^{-}$/*2*$^{-}$ cells was most similar to that of *mgp2*$^{-}$ cells and appears to abrogate the *mgp1*$^{-}$ slug phenotype, yet *mgp1*$^{-}$/*2*$^{-}$ cells still formed aberrant fruiting bodies whereas *mgp2*$^{-}$ cells did not. The reasons for this are clearly complicated, and as yet unclear. Motility is as much a part of development as it is of vegetative growth; thus the poor motility of cells is probably linked to the aberrant development of the mutants.

GFP-MEGAP1 localises to tubules of the contractile vacuole network in axenically growing cells. Presenting cells with a hypo-osmotic shock caused GFP-MEGAP1 to move predominantly into the cytosol. Transient localisation of GFP-MEGAP1 to the contractile vacuole ensued in a punctate fashion once emptying of vacuoles had begun (Fig. 7B), remaining bound as long as a tubule was present. This manner of localisation suggests that MEGAP1 is functioning in the tubulation of the contractile vacuole network. The sluggish expulsion of vacuoles in the *mgp1*$^{-}$/*2*$^{-}$ mutant would further suggest that the tubulating activity of the MEGAPs lends force to the expulsion process. The method by which contractile vacuoles 'contract' in *D. discoideum* is unclear. Deep-etch EM replicas reveal no F-actin or myosin present on the contractile vacuoles (Heuser, 2006) and as such no muscle-like contraction would be possible. It has been postulated (Clarke et al., 2002; Gerisch et al., 2002) that an asymmetry in the phospholipids of the contractile vacuole network provides the contractile mechanism. This hypothesis argues that filling of vacuoles places a strain on the membrane. The natural tendency of the vacuoles to be tubular then drives the emptying process. Our data suggest that, in addition to this, the tubulating activity of the F-BAR domain of the MEGAP proteins also adds a substantial factor of the force to the expulsion process.

The contractile vacuole network is drastically affected but still functional in *mgp1*$^{-}$/*2*$^{-}$ cells, suggesting either some redundancy of function between the four identified MEGAP proteins or compensation by the cell. Several proteins associated with the contractile vacuole network are related to human proteins, suggesting that functions of the contractile vacuole network have been preserved during the evolution of higher eukaryotes (Gerisch et al., 2002). In fact, the phenotypes observed in *D. discoideum* MEGAP mutants (i.e. motility, membrane association) are functionally similar to those reported for mammalian MEGAP (Endris et al., 2002; Soderling et al., 2002; Yang et al., 2006) and FBP17 (Itoh et al., 2005; Tsujita et al., 2006). In addition, our observations of the *S. cerevisiae Rgd* mutants also point to a role in vacuole regulation. The excessive vacuoles phenotype observed in both *Rgd1Δ* and *Rgd2Δ* mutants is consistent with the *mgp1*$^{-}$/*2*$^{-}$ null contractile vacuole phenotypes observed in *D. discoideum*. In addition to this, the abnormal behaviour of the vacuoles in these cell lines could be consistent with the *Rgd1Δ* mutant growth defect in minimal medium during entry into stationary phase (Barthe et al., 1998). Presumably, this unusual vacuole behaviour is detrimental to pH regulation; this is consistent with *RGD1* being transcribed in response to low-pH shock (Gatti et al., 2005). Unlike the mammalian homologues of MEGAP we find no evidence for an interaction with SCAR/WAVE.

We propose a model where MEGAP1 is intrinsic to the structural integrity of the tubular network of the contractile vacuole system (Fig. 10). Under normal growth conditions, the contractile vacuole is predominantly tubular. Binding of MEGAP1 acts as a mechanism for maintaining this tubularity (Fig. 10A). When the cell encounters hypo-osmotic conditions, water enters, and MEGAP1 detaches from the membrane – perhaps in response to a signal – allowing the tubule

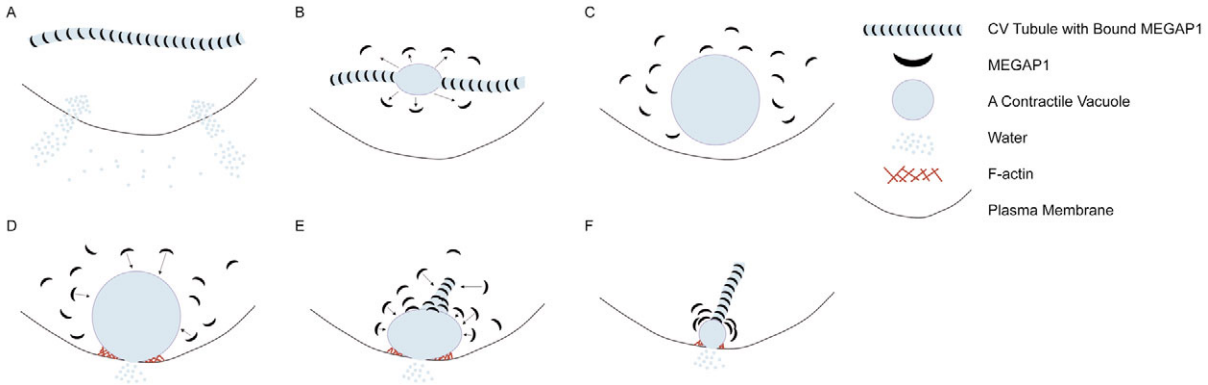

Fig. 10. Model of MEGAP1 function. (A) The contractile vacuole network is mostly tubular when MEGAP1 is bound. (B) As water enters the cell, MEGAP1 moves to the cytosol, allowing a vacuole to form. (C) The bladder grows until the vacuole has reached full size and requires emptying. (D) The contractile vacuole contacts the plasma membrane, forming a discrete pore (contained by a ring of F-actin) and begins to empty. MEGAP1 detects the change in curvature. (E) As the contractile vacuole empties, MEGAP1 binds, tubulating the bladder, adding force to the expulsion. (F) The bladder continues emptying and tubulating, and the cycle begins anew.

to fill like a bladder (Fig. 10B,C). Once the bladder is full, it moves to the membrane and a pore forms, initiating the expulsion process (Fig. 10D). As the bladder empties, MEGAP1 detects the changing curvature and begins to bind (Fig. 10D,E). Binding of MEGAP1 causes the bladder to retubulate, driving emptying (Fig. 10E,F), until the vacuole is tubular once more. We have shown that MEGAPs are important in a variety of cellular processes in *D. discoideum*. Specifically, MEGAP1 regulates tubulation of the contractile vacuole and represents a novel mechanism for supplying force to the vacuole expulsion process. Furthermore, the abnormal behaviour of vacuoles in the *S. cerevisiae* homologues *rgd1Δ* and *rgd2Δ* suggests that these roles are evolutionarily conserved.

Materials and Methods

Cell culture and development

D. discoideum cells were grown axenically in HL-5 medium at 22°C in Petri dishes or shaking flasks. For experiments requiring bacterially grown cells, *D. discoideum* were plated onto lawns of *Klebsiella aerogenes* on SMM agar and harvested after 72 hours by washing repeatedly in KK_2 buffer. For experiments requiring developed cells, *D. discoideum* were harvested, washed and starved for 1 hour by shaking 2×10^7 cells/ml in KK_2 buffer, then treated with 0.1 μM cAMP every 6 minutes for 4 hours while shaking.

Knockout constructs

D. discoideum homologues of MEGAP were identified by BLAST searches against the Tsukuba *Dictyostelium* cDNA database (Muramoto et al., 2003) and the *Dictyostelium* genome project libraries (Eichinger et al., 2005) using the FCH domain of mammalian MEGAP. *mgp1* (DictyBaseID DDB0188795) was cloned from cDNA (AHN288) into the *Hin*dIII/*Not*I sites of PCR Blunt TOPOII vector (Invitrogen). A blasticidin-resistance cassette was then cloned into the solitary *Eco*RI site of the gene. This construct was linearised using *Hin*dIII/*Not*I restriction enzymes and electroporated into *Dictyostelium* AX3 cell lines. Single clones of blasticidin-resistant transformants were obtained and screened by Southern hybridisation analysis.

mgp2 (dictyBaseID DDB0190747) was amplified from AX3 genomic DNA by 4-primer PCR to engineer a *Bam*HI site at position 1557-1563, a 5′ *Xba*I site and a 3′ *Xho*I site using the primers: 5′-TCCA**TCTAGA**ACCAAATTTAAATTCACA-GAT-3′ Upstream; 5′-GTCCAA**CTCGAG**CATTAAATCTTCACTTGATATG-3′ Downstream; 5′-AATG**GGATCC**ACTAGTAATTTAGCTATGGT-3′ Mid Forward; 5′-ACCATAGCTAAATTACTAGT**GGATCC**CATT-3′ Mid Reverse. The engineered restriction sites are highlighted in bold.

The resulting PCR product was cloned into PCR Blunt TOPOII vector (Invitrogen) and cloning either a blasticidin- or a hygromycin-resistance cassette into the *Bam*HI site in the gene made two different knockout constructs. These constructs were linearised with *Not*I/*Kpn*I restriction enzymes and electroporated into *Dictyostelium* AX3 cell lines. Single clones of transformants were obtained and screened by Southern hybridisation analysis. To create the *mgp1*$^-$/*mgp2*$^-$ double mutant, the hygromycin-resistant *mgp2*-null cells were transformed with the blasticidin disrupted *mgp1* construct. Colonies resistant to both blasticidin and hygromycin were screened by Southern hybridisation analysis.

Transformation

Transformation of *Dictyostelium* cells was performed by a modification of Howard et al. (Howard et al., 1998). Briefly, exponentially growing cells (~1.6×10^7 per zap) resuspended in electroporation buffer (10 mM potassium phosphate buffer, pH 6.1, 50 mM sucrose) were mixed with 10 μg linearised DNA and electroporated in a BioRad gene pulser at 1.0-1.2 kV, 3 mF with 5 Ω resistance in series. Following a 10 minute incubation on ice, the cells were incubated for 15 minutes at 22°C with 2 μl healing solution (100 mM $CaCl_2$, 100 mM $MgCl_2$) and then culture medium was added. Drugs for selection were added 24 hours after electroporation.

Under-agar chemotaxis

Under-agar chemotaxis of cells was studied using an adapted method (Laevsky and Knecht, 2001). To observe cAMP chemotaxis, a single trough (approximately 2 mm wide) was cut into a thin layer of 1% KK_2 agar containing 100 nM cAMP, which was excised from a plastic Petri dish and placed in a glass-bottomed dish. The trough was filled with 100 μl of developed log-phase cells at a density of approximately 1-2×10^7/ml. Cells were imaged using DIC microscopy.

Micropipette assay

Micropipette chemotaxis assays were carried out using a method adapted from Funamoto et al. (Funamoto et al., 2001). Briefly, developed cells were resuspended in KK_2 at a density of 5×10^4 cells/cm^2 and plated onto Willco 60 mm glass-bottomed dishes (thickness 0.17 mm). An Eppendorf micromanipulator 5171 with a glass capillary needle (Eppendorf FemtotipI™), filled with 1 μM cAMP solution was brought into the field of view of an inverted microscope. The capillary needle was attached to a FemtoJet™ microinjector with the compensation pressure set between 10 and 30 hPa to allow diffusion. The response of cells to the needle was viewed using a Zeiss Axiovert microscope set up for DIC microscopy. 400-frame time-lapse movies were captured at a rate of one frame every 3 seconds.

Phototaxis assay

Phototaxis assays were carried out as previously described (Darcy et al., 1994). Briefly, approximately 2×10^6 cells were placed as a 'clump' on the centre of charcoal agar plates (1% agar, 0.5% activated charcoal in dH_2O), sealed in a dark container and given a lateral light source. Phototaxis was scored after incubation for 48 hours at 22°C by comparing mutant strains to the wild-type parent strain.

Development on agar

2×10^7 cells were washed twice in KK_2 and spread on KK_2 agar containing 2 mM $MgCl_2$. Cells were left to adhere for 20 minutes then the liquid was removed and the plates incubated at 22°C.

Live-cell imaging

For all live-imaging experiments, cells were incubated with 1 mM Trolox C overnight prior to imaging.

For imaging of GFP-MEGAP1, axenically grown cells were adhered to glass-bottomed dishes (Willco-Dish, Willco Wells, Amsterdam, The Netherlands) and incubated in Lo Flo medium (ForMedium, Hunstanton, UK), for 2 hours to reduce autofluorescence. Cells were then incubated in one-third strength Lo Flo for 30 minutes to stimulate contractile vacuole activity. Immediately before imaging, cells were compressed under a thin layer of agar as described (Yumura et al., 1984). Images were obtained using a Bio-Rad Radiance 2000 MP confocal microscope. 40 or 80 frame time-lapse movies were captured at a rate of one frame per 6 seconds.

For FM2-10 observation, AX3 and *mgp*$^-$ cells were prepared as described previously except that the Lo Flo and agar contained 20 μg/ml FM2-10 (Molecular Probes). Images were obtained using a Leica TCS SP2 confocal microscope. 40 to 120 frame time-lapse movies were captured at a rate of one frame per 6 seconds.
For yeast FM4-64 experiments, early log-phase cells were incubated in YPD containing 40 mM FM4-64 (Molecular Probes) for 15 minutes at 30°C, then resuspended in fresh YPD medium and incubated for 20 minutes before mounting on slides. Images were captured using a Zeiss Axioskop2 microscope equipped with a Hamamatsu digital; camera C4742-95 and a 100× oil-immersion objective.

Fluid-phase uptake assays

Fluid-phase uptake was measured as described previously (Maniak et al., 1995). Samples (10 ml) of 5×10^6 cells/ml were shaken in 25 ml flasks at 150 r.p.m. TRITC (tetramethylrhodamine β-isothiocyanate)-dextran (Sigma) was added to a final concentration of 2 mg/ml. Samples of 1 ml were withdrawn at intervals and added to 100 μl Trypan Blue (Sigma) solution to quench extracellular fluorescence. Samples were centrifuged for 3 minutes at 500 ***g***. The cell pellet was washed once in 1 ml KK_2 buffer, resuspended in 1 ml KK_2 buffer, and relative intensity was immediately measured in a PTI fluorescence spectrometer at 544 nm for excitation and 574 nm for emission.

For live-cell imaging of fluid-phase uptake, axenically grown cells were adhered to glass-bottomed dishes (Willco) and incubated in Lo Flo medium containing 2 mg/ml TRITC-dextran for 30 minutes. Time-lapse images were captured using a Leica TCS SP2 confocal microscope. 40 to 120 frame time-lapse movies were captured at a rate of one frame per 10 seconds.

We are very grateful to both Margaret Clarke and Arturo De Lozanne for their help with all things contractile vacuole. We would like to thank all members of the Insall/Machesky labs for their constructive discussion of the results. We are very grateful as always to the Japanese cDNA project. R.H.I. is supported by an MRC Senior Research Fellowship. R.J.W.H. is supported by a Scientific Project Committee Studentship.

References

Aspenstrom, P. (1997). A Cdc42 target protein with homology to the non-kinase domain of FER has a potential role in regulating the actin cytoskeleton. *Curr. Biol.* **7**, 479-487.
Aspenstrom, P., Fransson, A. and Richnau, N. (2006). Pombe Cdc15 homology proteins: regulators of membrane dynamics and the actin cytoskeleton. *Trends Biochem. Sci.* **31**, 670-679.
Barrett, T., Xiao, B., Dodson, E. J., Dodson, G., Ludbrook, S. B., Nurmahomed, K., Gamblin, S. J., Musacchio, A., Smerdon, S. J. and Eccleston, J. F. (1997). The structure of the GTPase-activating domain from p50rhoGAP. *Nature* **385**, 458-461.
Barthe, C., de Bettignies, G., Louvet, O., Peypouquet, M. F., Morel, C., Doignon, F. and Crouzet, M. (1998). First characterization of the gene RGD1 in the yeast Saccharomyces cerevisiae. *C. R. Acad. Sci. III* **321**, 453-462.
Bear, J. E., Rawls, J. F. and Saxe, C. L. (1998). SCAR, a WASP-related protein, isolated as a suppressor of receptor defects in late Dictyostelium development. *J. Cell Biol.* **142**, 1325-1335.

Blagg, S. L., Stewart, M., Sambles, C. and Insall, R. H. (2003). PIR121 regulates pseudopod dynamics and SCAR activity in Dictyostelium. *Curr. Biol.* **13**, 1480-1487.
Clarke, M., Köhler, J., Arana, Q., Liu, T., Heuser, J. and Gerisch, G. (2002). Dynamics of the vacuolar H(+)-ATPase in the contractile vacuole complex and the endosomal pathway of Dictyostelium cells. *J. Cell Sci.* **115**, 2893-2905.
Coyle, I. P., Koh, Y. H., Lee, W. C., Slind, J., Fergestad, T., Littleton, J. T. and Ganetzky, B. (2004). Nervous wreck, an SH3 adaptor protein that interacts with Wsp, regulates synaptic growth in Drosophila. *Neuron* **41**, 521-534.
Darcy, P. K., Wilczynska, Z. and Fisher, P. R. (1994). Genetic analysis of Dictyostelium slug phototaxis mutants. *Genetics* **137**, 977-985.
Dumontier, M., Hocht, P., Mintert, U. and Faix, J. (2000). Rac1 GTPases control filopodia formation, cell motility, endocytosis, cytokinesis and development in Dictyostelium. *J. Cell Sci.* **113**, 2253-2265.
Eichinger, L., Pachebat, J. A., Glockner, G., Rajandream, M. A., Sucgang, R., Berriman, M., Song, J., Olsen, R., Szafranski, K., Xu, Q. et al. (2005). The genome of the social amoeba Dictyostelium discoideum. *Nature* **435**, 43-57.
Eitzen, G., Thorngren, N. and Wickner, W. (2001). Rho1p and Cdc42p act after Ypt7p to regulate vacuole docking. *EMBO J.* **20**, 5650-5656.
Endris, V., Wogatzky, B., Leimer, U., Bartsch, D., Zatyka, M., Latif, F., Maher, E. R., Tariverdian, G., Kirsch, S., Karch, D. et al. (2002). The novel Rho-GTPase activating gene MEGAP/ srGAP3 has a putative role in severe mental retardation. *Proc. Natl. Acad. Sci. USA* **99**, 11754-11759.
Faix, J., Clougherty, C., Konzok, A., Mintert, U., Murphy, J., Albrecht, R., Muhlbauer, B. and Kuhlmann, J. (1998). The IQGAP-related protein DGAP1 interacts with Rac and is involved in the modulation of the F-actin cytoskeleton and control of cell motility. *J. Cell Sci.* **111**, 3059-3071.
Fountain, S. J., Parkinson, K., Young, M. T., Cao, L., Thompson, C. R. and North, R. A. (2007). An intracellular P2X receptor required for osmoregulation in Dictyostelium discoideum. *Nature* **448**, 200-203.
Frost, A., De Camilli, P. and Unger, V. M. (2007). F-BAR proteins join the BAR family fold. *Structure* **15**, 751-753.
Funamoto, S., Milan, K., Meili, R. and Firtel, R. A. (2001). Role of phosphatidylinositol 3′ kinase and a downstream pleckstrin homology domain-containing protein in controlling chemotaxis in dictyostelium. *J. Cell Biol.* **153**, 795-810.
Gabriel, D., Hacker, U., Kohler, J., Muller-Taubenberger, A., Schwartz, J. M., Westphal, M. and Gerisch, G. (1999). The contractile vacuole network of Dictyostelium as a distinct organelle: its dynamics visualized by a GFP marker protein. *J. Cell Sci.* **112**, 3995-4005.
Gatti, X., de Bettignies, G., Claret, S., Doignon, F., Crouzet, M. and Thoraval, D. (2005). RGD1, encoding a RhoGAP involved in low-pH survival, is an Msn2p/Msn4p regulated gene in Saccharomyces cerevisiae. *Gene* **351**, 159-169.
Gerisch, G., Heuser, J. and Clarke, M. (2002). Tubular-vesicular transformation in the contractile vacuole system of Dictyostelium. *Cell Biol. Int.* **26**, 845-852.
Hacker, U., Albrecht, R. and Maniak, M. (1997). Fluid-phase uptake by macropinocytosis in Dictyostelium. *J. Cell Sci.* **110**, 105-112.
Heuser, J. (2006). Evidence for recycling of contractile vacuole membrane during osmoregulation in Dictyostelium amoebae-A tribute to Gunther Gerisch. *Eur. J. Cell Biol.* **85**, 859-871.
Heuser, J., Zhu, Q. and Clarke, M. (1993). Proton pumps populate the contractile vacuoles of Dictyostelium amoebae. *J. Cell Biol.* **121**, 1311-1327.
Ho, H. Y., Rohatgi, R., Lebensohn, A. M., Le, M., Li, J., Gygi, S. P. and Kirschner, M. W. (2004). Toca-1 mediates Cdc42-dependent actin nucleation by activating the N-WASP-WIP complex. *Cell* **118**, 203-216.
Howard, P. K., Ahern, K. G. and Firtel, R. A. (1998). Establishment of a transient expression system for Dictyostelium discoideum. *Nucleic Acids Res.* **16**, 2613-2623.
Ibarra, N., Blagg, S. L., Vazquez, F. and Insall, R. H. (2006). Nap1 regulates Dictyostelium cell motility and adhesion through SCAR-dependent and -independent pathways. *Curr. Biol.* **16**, 717-722.
Itoh, T., Erdmann, K. S., Roux, A., Habermann, B., Werner, H. and De Camilli, P. (2005). Dynamin and the actin cytoskeleton cooperatively regulate plasma membrane invagination by BAR and F-BAR proteins. *Dev. Cell* **9**, 791-804.
Kessels, M. M. and Qualmann, B. (2004). The syndapin protein family: linking membrane trafficking with the cytoskeleton. *J. Cell Sci.* **117**, 3077-3086.
Klionsky, D. J., Herman, P. K. and Emr, S. D. (1990). The fungal vacuole: composition, function, and biogenesis. *Microbiol. Rev.* **54**, 266-292.
Laevsky, G. and Knecht, D. A. (2001). Under-agarose folate chemotaxis of Dictyostelium discoideum amoebae in permissive and mechanically inhibited conditions. *Biotechniques* **31**, 1140-1142, 1144, 1146-1149.
Letunic, I., Copley, R. R., Pils, B., Pinkert, S., Schultz, J. and Bork, P. (2006). SMART 5, domains in the context of genomes and networks. *Nucleic Acids Res.* **34**, D257-D260.
Lippincott, J. and Li, R. (2000). Involvement of PCH family proteins in cytokinesis and actin distribution. *Microsc. Res. Tech.* **49**, 168-172.
Maniak, M., Rauchenberger, R., Albrecht, R., Murphy, J. and Gerisch, G. (1995). Coronin involved in phagocytosis: dynamics of particle-induced relocalization visualized by a green fluorescent protein Tag. *Cell* **83**, 915-924.
Modregger, J., Ritter, B., Witter, B., Paulsson, M. and Plomann, M. (2000). All three PACSIN isoforms bind to endocytic proteins and inhibit endocytosis. *J. Cell Sci.* **113**, 4511-4521.
Muramoto, T., Suzuki, K., Shimizu, H., Kohara, Y., Kohriki, E., Obara, S., Tanaka, Y. and Urushihara, H. (2003). Construction of a gamete-enriched gene pool and RNAi-mediated functional analysis in Dictyostelium discoideum. *Mech. Dev.* **120**, 965-975.
Peter, B. J., Kent, H. M., Mills, I. G., Vallis, Y., Butler, P. J., Evans, P. R. and McMahon, H. T. (2004). BAR domains as sensors of membrane curvature: the amphiphysin BAR structure. *Science* **303**, 495-499.
Qualmann, B., Roos, J., DiGregorio, P. J. and Kelly, R. B. (1999). Syndapin I, a synaptic dynamin-binding protein that associates with the neural Wiskott-Aldrich syndrome protein. *Mol. Biol. Cell* **10**, 501-513.
Roumanie, O., Weinachter, C., Larrieu, I., Crouzet, M. and Doignon, F. (2001). Functional characterization of the Bag7, Lrg1 and Rgd2 RhoGAP proteins from Saccharomyces cerevisiae. *FEBS Lett.* **506**, 149-156.
Schultz, J., Milpetz, F., Bork, P. and Ponting, C. P. (1998). SMART, a simple modular architecture research tool: identification of signaling domains. *Proc. Natl. Acad. Sci. USA* **95**, 5857-5864.
Soderling, S. H., Binns, K. L., Wayman, G. A., Davee, S. M., Ong, S. H., Pawson, T. and Scott, J. D. (2002). The WRP component of the WAVE-1 complex attenuates Rac-mediated signalling. *Nat. Cell Biol.* **4**, 970-975.
Soderling, S. H., Langeberg, K. L., Soderling, J. A., Davee, S. M., Simerly, R., Raber, J. and Scott, J. D. (2003). Loss of WAVE-1 causes sensorimotor retardation and reduced learning and memory in mice. *Proc. Natl. Acad. Sci. USA* **100**, 1723-1728.
Soderling, S. H., Guire, E. S., Kaech, S., White, J., Zhang, F., Schutz, K., Langeberg, L. K., Banker, G., Raber, J. and Scott, J. D. (2007). A WAVE-1 and WRP signaling complex regulates spine density, synaptic plasticity, and memory. *J. Neurosci.* **27**, 355-365.
Soulard, A., Lechler, T., Spiridonov, V., Shevchenko, A., Shevchenko, A., Li, R. and Winsor, B. (2002). Saccharomyces cerevisiae Bzz1p is implicated with type I myosins in actin patch polarization and is able to recruit actin-polymerizing machinery in vitro. *Mol. Cell. Biol.* **22**, 7889-7906.
Tsujita, K., Suetsugu, S., Sasaki, N., Furutani, M., Oikawa, T. and Takenawa, T. (2006). Coordination between the actin cytoskeleton and membrane deformation by a novel membrane tubulation domain of PCH proteins is involved in endocytosis. *J. Cell Biol.* **172**, 269-279.
Vlahou, G. and Rivero, F. (2006). Rho GTPase signaling in Dictyostelium discoideum: insights from the genome. *Eur. J. Cell Biol.* **85**, 947-959.
Wong, K., Ren, X., Huang, Y., Xie, Y., Liu, G., Saito, H., Tang, H., Wen, L., Brady-Kalnay, S. and Mei, L. (2001). Signal transduction in neuronal migration: roles of GTPase activating proteins and the small GTPase Cdc42 in the Slit-Robo pathway. *Cell* **107**, 209-221.
Yang, Y., Marcello, M., Endris, V., Saffrich, R., Fischer, R., Trendelenburg, M. F., Sprengel, R. and Rappold, G. (2006). MEGAP impedes cell migration via regulating actin and microtubule dynamics and focal complex formation. *Exp. Cell Res.* **312**, 2379-2393.
Yumura, S., Mori, H. and Fukui, Y. (1984). Localization of actin and myosin for the study of ameboid movement in Dictyostelium using improved immunofluorescence. *J. Cell Biol.* **99**, 894-899.
Zimmermann, K., Opitz, N., Dedio, J., Renne, C., Muller-Esterl, W. and Oess, S. (2002). NOSTRIN: a protein modulating nitric oxide release and subcellular distribution of endothelial nitric oxide synthase. *Proc. Natl. Acad. Sci. USA* **99**, 17167-17172.